Journal of Ceramic Processing Research. Vol. 22, No. 1, pp. 8~15 (2021)
(Received 21 January 2020, Received in revised form 30 April 2020, Accepted 10 June 2020)
https://doi.org/10.36410/jcpr.2021.22.1.8

J O U R N A L O F
Ceramic Processing Research

Preparation and luminescent properties of Tb^{3+}/Sm^{3+} co-doped phosphate glasses for display device applications

Qian Zhang[a,b], Lei Han[b], Weizhen Liu[b], Weixiong You[b], Anxian Lu[a,*] and Zhiwei Luo[a]
[a]*School of Materials Science and Engineering, Central South University, Changsha 410083, China*
[b]*Faculty of Materials Metallurgy and Chemistry, Jiangxi University of Science and Technology, Ganzhou 341000, China*

Development of orange light emitting materials cannot be ignored. In this paper, a novel Tb^{3+}/Sm^{3+} co-doped P_2O_5-SrO-BaO-ZnO-glasses have been prepared. The prepared glasses consisted predominantly of Q^2 units, and a small amount of Q^0 and Q^1 units. For absorption spectra of glasses, eight obvious absorption bands were found. Under the excitation of 402 nm and 374 nm xenon lamp, the emission spectra and fluorescence lifetimes of glasses showed big difference. Under the excitation of 374 nm xenon lamp, there was significant energy transfer process between Sm^{3+} and Tb^{3+} ions in glasses. The fluorescence decay curves conformed to a double-exponential decay function, the average fluorescence lifetimes of glasses G02 ~ G10 were 2.38 ms, 2.67 ms, 1.96 ms, 1.81 ms, and 1.61 ms with the increasing of Sm_2O_3 content, and the glasses emitted a distinct orange light. The distinctive properties indicate that this system glass has potential applications in display devices.

Keywords: Phosphate glasses, Tb^{3+}/Sm^{3+} co-doped, Orange light, Luminescence.

Introduction

Rare-earth (RE) luminescent materials are one of the core materials of current lighting, display and information detection devices, and are also indispensable materials for the development of new generation lighting and display technologies in the future [1]. Due to its excellent luminescence properties, RE ions-doped luminescent materials have a wide range of potential applications in white LEDs, display devices, solar cells, lasers and optical temperature sensors [2-5], and have attracted widespread attention from researchers around the world. Compared with other luminescent materials, luminescent glass has many excellent properties, such as transparency, uniformity, low cost, easy processing, as well as it is also an excellent RE ion matrix material [6]. Therefore, the research on RE doped luminescent glass has important scientific significance and application value.

In the past few decades, many RE doped luminescent materials have been studied, such as Eu^{3+} [7], Er^{3+} [8], Sm^{3+} [9], Tb^{3+} [10], Dy^{3+} [11] doped glasses, etc. Among various RE ions doped matrix materials, Tb^{3+}/Sm^{3+} co-doped glass can be used as a good activator due to its unique spectral characteristics, rich emission intensity, and energy transfer from Tb^{3+} to Sm^{3+}. At present, research on RE ions doped luminescent glass materials has mainly focused on oxyfluoride, sulfide, silicate, and aluminum borosilicate matrix systems. However, the research on RE ions doped phosphate luminescent glass is still scarce. It is well known that the luminescence characteristics of RE ions in glass depend on the chemical compositions, structure and properties of the host glass. Among them, phosphate glass is considered to be a good matrix material doped with RE ions, because of its good optical properties, moderate phonon energy, lower melting temperature, low refractive index, dispersion, as well as high doping concentrations, etc. Unfortunately, the stability of pure phosphate glasses is poor, which limits their practical application. Therefore, it is an effective method to add some other oxides to pure phosphate glass for improving the structural stability of glass. It has been reported that adding ZnO to pure phosphate glass can improve the stability of the glass [12, 13]. Zn^{2+} ions act as a network former in phosphate glass, so it can form either $[ZnO_4]$ tetrahedron or P-O-Zn through ionic cross-linking, thereby integrating the glass network and improving its chemical stability. In addition, adding SrO to phosphate glass can form a metaphosphate structure, which is beneficial to improve the structural stability of glass [14]. In view of this, this work will consider the incorporation of ZnO, SrO, and BaO into pure phosphate glass to improve the thermal stability and increase the application range of glass.

In this paper, Tb^{3+}/Sm^{3}+ co-doped P_2O_5-ZnO-SrO-BaO luminescent glasses were prepared. The influence of chemical composition and structure on the luminescence properties of the glass (emission intensity, fluorescence lifetimes, chromaticity coordinates and correlate color temperature, etc.) was studied, and the transition and

*Corresponding author:
Tel : +86 0731 88877057
Fax: +86 0731 88877057
E-mail: axlu@mail.csu.edu.cn

luminescence mechanisms of the excitation energy levels of RE doped glasses were explored.

Experimental Procedures

Materials preparation

The strontium carbonate ($SrCO_3 \geq 99.0\%$), barium carbonate ($BaCO_3 \geq 99.0\%$), zinc oxide ($ZnO \geq 99.0\%$), and diammonium phosphate ($(NH_4)_2HPO_4 \geq 99.0\%$) were purchased from Xilong Chemical Co. Ltd., China. The antimony trioxide (Sb_2O_3) was purchased from Sinopharm Chemical Reagent Co. Ltd., China. The tetraterbium heptaoxide ($Tb_4O_7 \geq 99.99\%$) and samarium oxide ($Sm_2O_3 \geq 99.99\%$) were purchased from Ganzhou Jinyi New materials Co. Ltd., China. All chemicals were used without further purification.

The Tb^{3+}/Sm^{3+} co-doped phosphate glasses were prepared by the melt-quenching method, and the molar compositions of glasses with different Tb^{3+}/Sm^{3+} are given in Table 1. The raw materials were thoroughly mixed and then filled in the platinum crucible. Subsequently, the platinum crucible containing the mixture was heated at 1,300 ºC for 2 h in a furnace. Then, the melts were poured onto a preheated stainless-steel plate and later annealed at 400 ºC for 10 h in another furnace to release internal stress.

Characterization

Amorphous nature of glasses was identified by X-ray diffraction(XRD, MiniFlex 600, Rigaku, Japan) using Cu Kα radiation at a scanning velocity of 10º/min between diffraction angles (2θ) from 10 to 80º for all powder samples. The IR spectra of glasses were measured by using Fourier transform infrared spectrophotometer (FTIR, Nicolet 6700, USA) at room temperature with the wavenumber range of 400-4,000 cm^{-1}. The absorption spectra of glasses were measured with the UV spectrophotometer (SP-756P, Shanghai). The densities of glasses were tested by the Archimedes method using distilled water as the medium. The emission spectra and fluorescence decay curves of glasses were measured by spectrofluorometer (FLS 1000, Edingburgh Instruments, UK) pumped by 450 W xenon lamp at room temperature. The chromaticity coordinates (x, y) of glasses were calculated based on emission spectra by using software CIE1931.

Table 1. The mole composition of glasses with different Sm_2O_3 contents.

Sample numbers	Nominal composition (mol.%)	RE contents (external doping, mol.%)		[O]/[P] molar ratio
		Tb_2O_3	Sm_2O_3	
G02	45 P2O5-15 SrO-15 BaO-25 ZnO	0.5	0.2	3.1344
G04		0.5	0.4	3.1411
G06		0.5	0.6	3.1478
G08		0.5	0.8	3.1544
G10		0.5	1.0	3.1611

Results and Discussion

Glass characterization

Fig. 1 shows the typical XRD patterns of the Tb^{3+}/Sm^{3+} co-doped phosphate glasses G02 ~ G10. There was no characteristic peak that corresponded to any crystalline phase, implying that the obtained samples are all amorphous state.

FTIR spectra analysis

The IR spectra of glasses were investigated for identifying the variation of chemical bonds. As shown in Fig. 2, seven characteristic absorption bands around 517 cm^{-1}, 751 cm^{-1}, 917 cm^{-1}, 1,110 cm^{-1}, 1,620 cm^{-1}, 2,364 cm^{-1} and 3,425 cm^{-1} were found in IR spectra of glasses G02 ~ G10 in the wavenumber range of 400-4,000 cm^{-1}.

As shown in Fig. 2, the characteristic bands around 517 cm^{-1} were attributed to the bending vibration of O=P–O bands in Q^0 units [15]. The absorption bands at

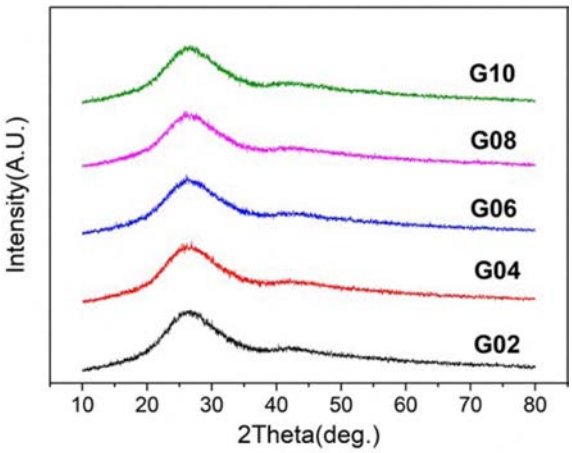

Fig. 1. X-ray diffraction patterns of Tb^{3+}/Sm^{3+} co-doped phosphate glasses.

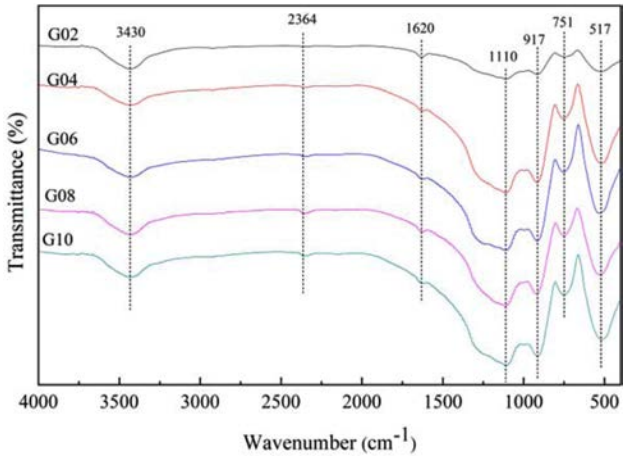

Fig. 2. FTIR spectra of Tb^{3+}/Sm^{3+} co-doped phosphate glasses.

~ 751 cm^{-1} were ascribed to the symmetric stretching vibration of P–O–P bonds in Q^2 units [14]. The bands located at ~ 917 cm^{-1} may be caused by the asymmetric stretching vibration of P–O–P bonds in Q^2 units [16], while the absorption bands near 1110 cm^{-1} may be caused by the asymmetric stretching modes of $(PO_3)^{2-}$ groups associated with Q^1 phosphate units [17]. The absorption bands near 1,620 cm^{-1} were ascribed to the bending vibrations of O–H bonds or stretching vibrations of P–O–H groups [18], as well as the characteristic bands around 2,364 cm^{-1} and 3,430 cm^{-1} may be assigned to the stretching vibration of O–H groups [19] and the symmetric stretching of the O–H bonds [20], respectively. This may be caused by the incorporation of water molecules during the sample preparation. Besides, the detailed vibration types of different wavenumbers in IR spectra are listed in Table 2.

Considering the measurement errors, the wavenumber of the absorption bands in IR spectra did not have significant changes although the Sm_2O_3 content increased. However, the intensity of absorption peak at ~ 517, 751, 917 cm^{-1} increased with the increasing of Sm_2O_3 content, which indicates that the contents of Q^0 and Q^2 units increased to some extent.

In order to identify the distribution of phosphate groups in the phosphate glass, the O/P molar ratio have been used by many investigator [12]. In this paper, the O/P ratio increased from 3.1344 to 3.1611, which is in the range of 3.0 ~ 3.5. According to the Ref. [12], for $2.5 \leq O/P < 3$, $O/P = 3.0$, $3 < O/P < 3.5$, $O/P = 3.5$ and $3.5 < O/P < 4.0$, glass structure is mainly composed of ultraphosphate groups (Q^3), metaphosphate groups (Q^2), polyphosphate units (Q^2, Q^1), pyrophosphate groups (Q^1) and orthophosphate units (Q^0), respectively. Consequently, this phosphate glass theoretically consists predominantly of polyphosphate units. However, it can be seen from Fig. 2 that the orthophosphate units (Q^0) were presented in the glass network, which is mainly due to the disproportionation reaction between the groups [21]:

$$2Q^1 \Leftrightarrow Q^0 + Q^2 \quad (1)$$

In view of this, it can be concluded that this glass consists predominantly of Q^2 units, along with minor Q^1 and Q^0 units. With the increasing of Sm_2O_3 content, the content of Q^1 structural units increases, while the Q^2 structural units decreases. Besides, the bond length and bond angle of P-O-P in glass structure also change.

3.3 Physical properties

The interdependence in density (ρ) and molar volume (V_m) with Sm_2O_3 content is shown in Fig. 3. For the densities of glasses G02 ~ G10, they were 3.513 g/cm^3, 3.528 g/cm^3, 3.547 g/cm^3, 3.561 g/cm^3 and 3.584 g/cm^3, respectively. It can be seen that density monotonically increased with the increasing of Sm_2O_3 content, which may be due to the molecular mass of Sm_2O_3 is greater. In addition, a monotonic decrease in the molar volume can be seen, which is most likely due to the constriction of glass structure. A similar phenomenon can be found in other references [22, 23].

3.4 Absorption spectra

The research on optical absorption is helpful to understand the optical induced transition of glass materials. In this paper, the absorption spectra of glasses G02 ~ G10 have been investigated. Fig. 4 depicts the absorption spectra of glasses in the wavelength of 330 nm to 900 nm. As shown in Fig. 4, it can be found that there were eight obvious absorption bands in the wavelength of 300-500 nm for each glass. Based on the Refs.[24, 25], these eight obvious absorption bands, around 344 nm, 361 nm, 374 nm, 402 nm, 415 nm, 462 nm, 470 nm, and 475 nm, can be assigned to the electron transition from ground level to excited levels: $^6F_{5/2} \rightarrow {}^4D_{7/2}$, $^6H_{5/2} \rightarrow {}^4D_{3/2}$, $^6H_{5/2} \rightarrow {}^6P_{7/2}$, $^6H_{5/2} \rightarrow {}^5P_{3/2}$, $^6H_{5/2} \rightarrow {}^6P_{5/2}$, $^6H_{5/2} \rightarrow {}^4I_{13/2}$, $^6H_{5/2} \rightarrow {}^4M_{15/2}$, and $^6H_{5/2} \rightarrow {}^4I_{11/2}$, respectively. As a whole the intensity of absorption bands gradually

Table 2. Detailed vibration types of different absorption bands.

Absorption bands (cm^{-1})	Vibration types
~ 517	Bending vibration of O=P–O bands in Q^0 units
~ 751	Symmetric stretching vibration of P–O–P bonds in Q^2 units
~ 917	Asymmetric stretching vibration of P–O–P bonds in Q^2 units
~ 1,110	Asymmetric stretching modes of $(PO_3)^{2-}$ groups in Q^1 units
~ 1,620	Bending vibrations of O–H bonds or stretching vibrations of P–O–H groups
~ 2,364	Stretching vibration of O–H groups
~ 3,430	Symmetric stretching of the O–H bonds

[Q^n is the conventional notation for phosphate groups in glass, where n (n = 0-3) is the number of bridging oxygen per PO_4 tetrahedron]

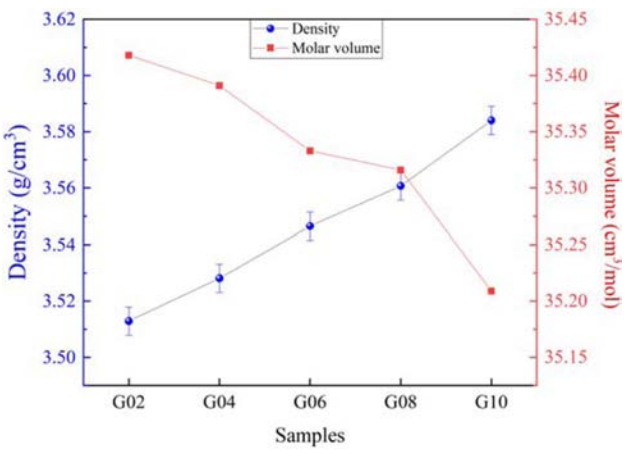

Fig. 3. Variation in density and molar volume Tb^{3+}/Sm^{3+} co-doped phosphate glasses.

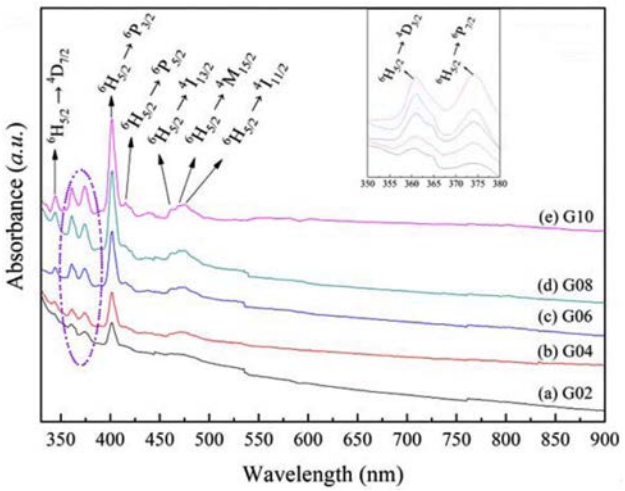

Fig. 4. Absorption spectra of Tb^{3+}/Sm^{3+} co-doped phosphate glasses.

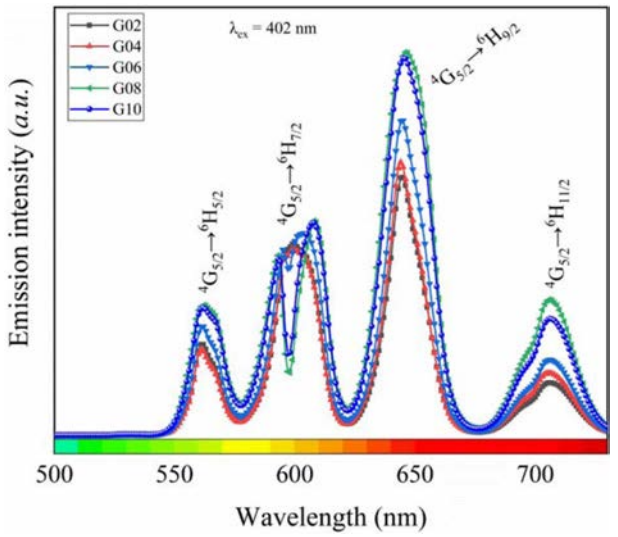

Fig. 5. Emission spectra of Tb^{3+}/Sm^{3+} co-doped phosphate glasses excited by 402 nm xenon lamp.

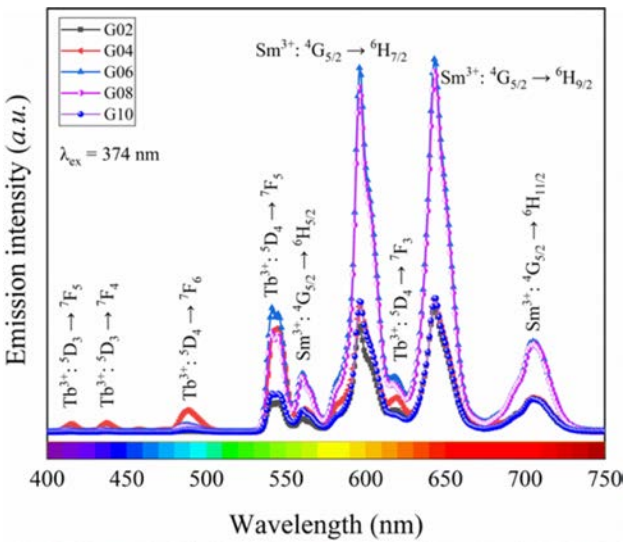

Fig. 6. Emission spectra of Tb^{3+}/Sm^{3+} co-doped phosphate glasses excited by 374 nm xenon lamp.

ascended with the Sm^{3+} content increasing, and the absorption bands located at 374 nm and 402 nm have strong intensity. In view of this, this system glass with different Sm_2O_3 contents can be excited effectively by the 394 nm and 402 nm light.

3.5 Emission spectra

Based on the results of absorption spectra, the Tb^{3+}/Sm^{3+} co-doped phosphate glasses were excited by 402 nm and 374 nm xenon lamp, and the emission spectrum for each glass are presented in Fig. 5 and Fig. 6. As shown in Fig. 5, the emission spectra excited by 402 nm xenon lamp showed four obvious peaks, which is ascribed to the transitions of Sm^{3+} [26, 27]: $^4G_{5/2} \rightarrow {}^6H_{5/2}$ (561 nm), $^4G_{5/2} \rightarrow {}^6H_{7/2}$ (599 nm), $^4G_{5/2} \rightarrow {}^6H_{9/2}$ (645 nm), and $^4G_{5/2} \rightarrow {}^6H_{11/2}$ (706 nm), respectively. Among these emission peaks, the emission peak belonging to the $^4G_{5/2} \rightarrow {}^6H_{9/2}$ transition was strongest than others. On the other hands, the intensity of emission peak gradually increased with the increasing of Sm_2O_3 content, and the peaks intensity reached the maximum as the content of Sm_2O_3 was 0.8 mol.%, and then the peaks intensity decreased, which may be caused by the cross-relaxation of Sm^{3+}. In addition, the emission peak attributed to the $^4G_{5/2} \rightarrow {}^6H_{7/2}$ transition appeared Stark splitting, the emission peaks split into two sharp peaks, which may be due to the changes of environment around Sm^{3+} ions in glasses. However, there were no the emission peaks of Sm^{3+}, which indicates that Tb^{3+} and Sm^{3+} cannot be effectively excited simultaneously by 402 nm light, and there was no energy transfer between Tb^{3+} and Sm^{3+}.

In view of this, the Tb^{3+}/Sm^{3+} co-doped phosphate glasses were excited by 374 nm xenon lamp, and the emission spectra of glass are depicted in Fig. 6. As shown in Fig. 6, the emission spectra showed nine obvious peaks. Based on the Refs. [28, 29], they are attributed to the transitions of $Tb^{3+}$and Sm^{3+}: $^5D_3 \rightarrow {}^7F_5$ (415 nm), $^5D_3 \rightarrow {}^7F_4$ (436 nm), $^5D_4 \rightarrow {}^7F_6$ (488 nm), $^5D_4 \rightarrow {}^7F_5$ (541 nm), $^4G_{5/2} \rightarrow {}^6H_{5/2}$ (561 nm), $^4G_{5/2} \rightarrow {}^6H_{7/2}$ (597 nm), $^5D_4 \rightarrow {}^7F_3$ (618 nm), $^4G_{5/2} \rightarrow {}^6H_{9/2}$ (643 nm), and $^4G_{5/2} \rightarrow {}^6H_{11/2}$ (704 nm), respectively. Among these emission peaks, the emission peak assigned to the $^4G_{5/2} \rightarrow {}^6H_{9/2}$ transition was strongest than others, which is very different from the data reported in other literatures [26, 28]. Interestingly, the intensity of $^5D_4 \rightarrow {}^7F_5$ transition was much greater than that of the $^4G_{5/2} \rightarrow {}^6H_{9/2}$ transition in other literatures, However, the opposite is true in this work. The intensity of emission peaks increased firstly and then decreased with increased in Sm_2O_3 content, and the peaks intensity reached maximum as the Sm_2O_3 content was 0.6 mol.%. Compared with the emission spectra excited by 402 nm xenon lamp, the emission

spectra were quite different. On the one hand, there were obvious emission peaks of Tb^{3+} in emission spectra, and these emission peaks are different from those of glass singly doped Tb^{3+} [30], which is due to the energy transfer of Tb^{3+} and Sm^{3+} in this glass system, suggesting that Tb^{3+} ions can have a sensitizing effect on the Sm^{3+} emission through a $Tb^{3+} \rightarrow Sm^{3+}$ energy transfer process [31]. On the other hand, the emission peaks attributed to the $^4G_{5/2} \rightarrow {}^6H_{7/2}$ transition did not appear Stark splitting, which may be related to the interaction effect between Tb^{3+} and Sm^{3+}, and the special structure of glass materials.

Fig. 7 portrays the energy level scheme of the emission with 374 nm excitation wavelength for the ET process from Tb^{3+} to Sm^{3+} ions. Two non-radiative transitions of $^5D_3 \rightarrow {}^5D_4$ (Tb^{3+} ions) and $^6P_{7/2} \rightarrow {}^4G_{7/2}$ (Sm^{3+} ions) were presented within the energy level scheme. Under the excitation of 394 nm light, the electrons of Tb^{3+} and Sm^{3+} ions are excited from the ground state ($^7F_6$ and $^6H_{5/2}$) to excited level ($^5D_3$ and $^6P_{7/2}$), respectively. Part of the electrons of Tb^{3+} ions in the $^5D_3$ directly get to $^7F_4$ and $^7F_5$ by radiative relaxation, and the other electrons relax up to the $^5D_3$ through non-radiative relaxation. Finally, the electrons of $^5D_4$ level get to the $^7F_3$, $^7F_5$, and $^7F_6$ levels, corresponding to 618 nm, 541 nm, 448 nm, by radiative relaxation. On the other hand, the 561 nm, 597 nm, 643 nm, and 704 nm emissions occur, respectively, via the $^4G_{5/2} \rightarrow {}^6H_{5/2}$, $^4G_{5/2} \rightarrow {}^6H_{7/2}$, $^4G_{5/2} \rightarrow {}^6H_{9/2}$, and $^4G_{5/2} \rightarrow {}^6H_{11/2}$ transitions of Sm^{3+} ions. In addition, upon excitation at 374 nm, the energy transfer processes between Tb^{3+} to Sm^{3+} ions can be described by the following pathways (as shown in Fig. 7) [26]:

ET1: $^5D_3(Tb^{3+}) + {}^6H_{5/2}(Sm^{3+}) \rightarrow {}^7F_4(Tb^{3+}) + {}^4M_{17/4}(Sm^{3+})$
ET2: $^5D_4(Tb^{3+}) + {}^6H_{5/2}(Sm^{3+}) \rightarrow {}^7F_6(Tb^{3+}) + {}^4I_{9/2}(Sm^{3+})$
ET3: $^5D_4(Tb^{3+}) + {}^6H_{5/2}(Sm^{3+}) \rightarrow {}^7F_6(Tb^{3+}) + {}^4G_{7/2}(Sm^{3+})$

Fluorescence lifetime

In order to study the nature of the energy transfer process, the fluorescence decay lifetimes all glasses were analyzed. Fig. 8 shows the fluorescence decay lifetimes all glasses excited by 402 nm and monitored at 645 nm (Sm^{3+}: $^4G_{5/2} \rightarrow {}^6H_{9/2}$). The all fluorescence decay curves can be described in the framework of tri-exponential approximation. Based on the Ref. [32], the

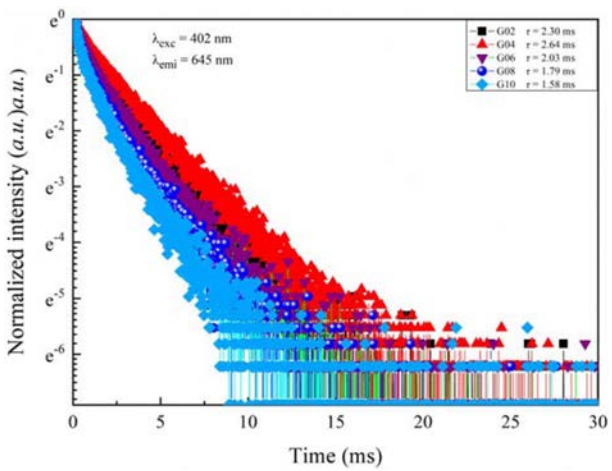

Fig. 8. Fluorescence decay curves of Tb^{3+}/Sm^{3+} co-doped phosphate glasses excited by 402 nm xenon lamp.

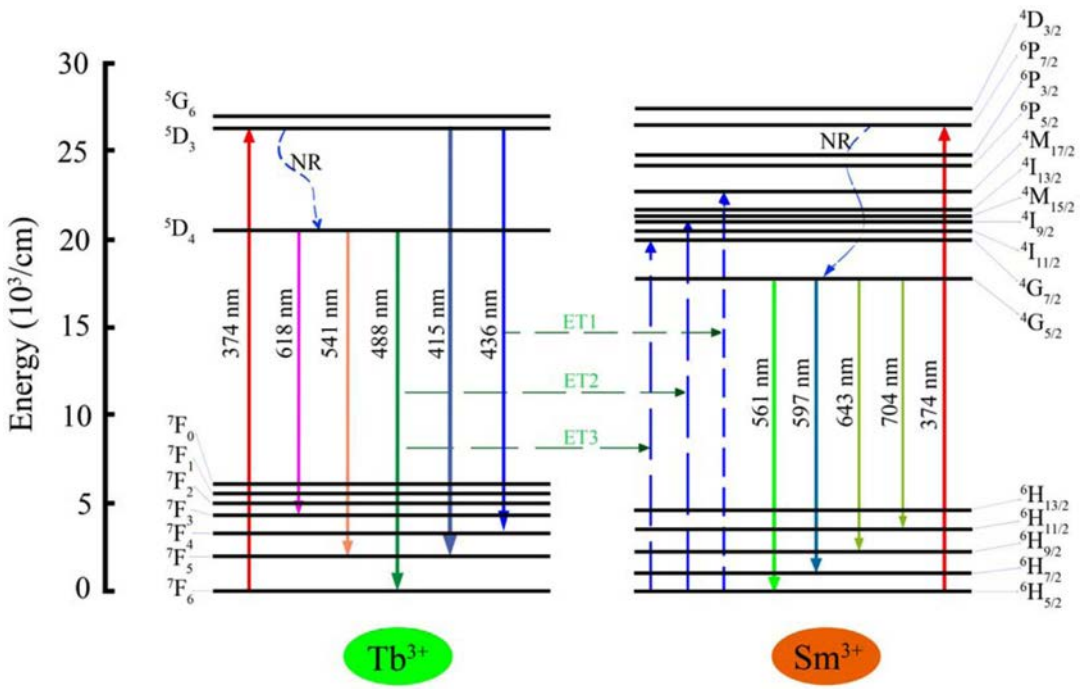

Fig. 7. Energy level diagram and energy transfer sketch map of Tb^{3+}/Sm^{3+} ions in glasses excited by 374 nm xenon lamp.

average fluorescence decay lifetimes of all glasses can be calculated by following equation:

$$\tau_{exp}=\frac{B_1\tau_1^2+B_2\tau_2^2+B_3\tau_3^2}{B_1\tau_1+B_2\tau_2+B_3\tau_3} \quad (2)$$

where τ_1, τ_2 and τ_3 are components of lifetimes; B_1, B_2 and B_3 are three constants of fitting.

According to Eq. (2), the average fluorescence lifetimes of phosphate glasses co-doped Tb^{3+}/Sm^{3+} were 2.30 ms, 2.64 ms, 2.03 ms, 1.79 ms, and 1.58 ms, respectively. It can be found that the average fluorescence lifetimes for all glasses first increased and then decreased with increase in Sm_2O_3 content, which may be caused by multi-phonon relaxation process and cross-relaxation energy transfer mechanism between two neighboring Sm^{3+} ions.

The fluorescence decay curves for all glasses excited by 374 nm and monitored at 643 nm are presented in Fig. 9. Here, all decay curves exhibited a tendency of increasing first and then decreasing with the increasing of Sm_2O_3 content. Different from the fluorescence decay curves excited by 402 nm xenon lamp, these curves all conformed to a double-exponential decay function. This is a common phenomenon in glass matrix. To calculate the average fluorescence lifetimes under $^4G_{5/2} \rightarrow {}^6H_{9/2}$ transition, the Eq. (2) can be used.

Based on Eq. (2), the calculated average fluorescence lifetimes of glasses were 2.38 ms, 2.67 ms, 1.96 ms, 1.81 ms, and 1.61 ms, respectively. It is observed that the average fluorescence lifetimes increased firstly and then decreased with increase in Sm_2O_3 content. Compared with the fluorescence lifetimes obtained under 402 nm light excitation, they had the same variation tendency, but the maximum of fluorescence lifetime was slightly greater than that obtained under 402 nm light excitation, which indicates that energy transition occurs between Tb^{3+} and Sm^{3+} ions in glasses.

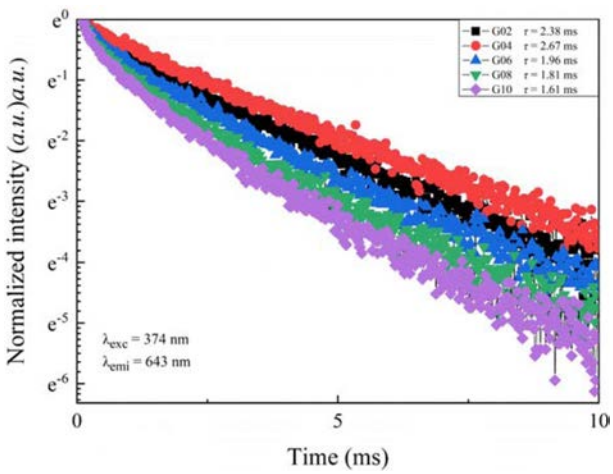

Fig. 9. Fluorescence decay curves of Tb^{3+}/Sm^{3+} co-doped phosphate glasses excited by 374 nm xenon lamp.

CIE chromaticity coordinates and correlated color temperature

Generally, the visible luminescence characteristics of glasses are estimated by means of chromaticity coordinates, which can help human to identify the original dichromatic composition of color. The chromaticity coordinates of glasses excited by 402 nm xenon lamp were calculated via CIE 1931 chromaticity diagram (as shown in Fig. 10). The chromaticity coordinates (x, y) of all glass were in the range of 0.5985 ~ 0.6062 and 0.3917 ~ 0.4006. From the Fig. 10 and Table 3, it can be observed that all glasses emit orange color. The correlated color temperature (CCT) is a specification of the color appearance of light emitted by a lamp, Table 3 lists the CCTs of all Tb^{3+}/Sm^{3+} co-doped glasses. As shown in Table 3, the CCTs of all glasses were in the range of 1,711 ~ 1,728 K. Fig. 11 shows the chromaticity coordinates of glasses excited by 374 nm xenon lamp, and the CCTs of all glass are listed in Table 4. From the Fig. 11 and Table 4, the chromaticity coordinates

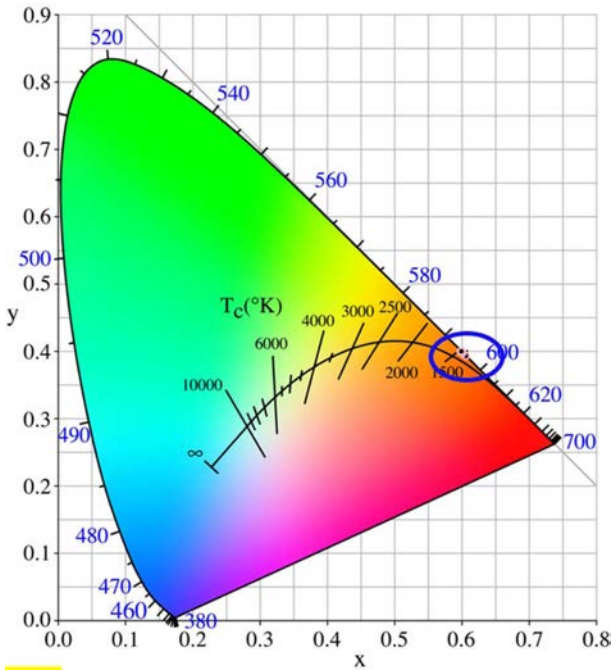

Fig. 10. Chromaticity CIE diagram of Tb^{3+}/Sm^{3+} co-doped phosphate glasses excited by 402 nm xenon lamp.

Table 3. Chromaticity coordinates and correlate color temperatures of Tb^{3+}/Sm^{3+} co-doped glasses excited by 402 nm xenon lamp.

Samples	Chromaticity coordinates		CCT (K)	Color of light emission
	x	y		
G02	0.6023	0.3969	1716	Orange
G04	0.6062	0.3930	1728	Orange
G06	0.6019	0.3917	1715	Orange
G08	0.5985	0.4006	1710	Orange
G10	0.5998	0.3994	1711	Orange

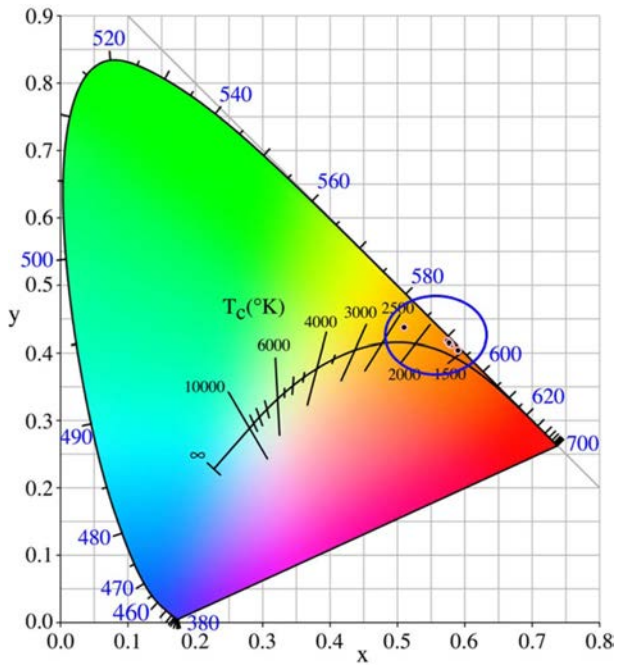

Fig. 11. Chromaticity CIE diagram of Tb^{3+}/Sm^{3+} co-doped phosphate glasses excited by 374 nm xenon lamp.

Table 4. Chromaticity coordinates and correlate color temperatures of Tb^{3+}/Sm^{3+} co-doped glasses excited by 374 nm xenon lamp.

Samples	Chromaticity coordinates		CCT (K)	Color of light emission
	x	y		
G02	0.5910	0.4043	1713	Orange
G04	0.5111	0.4374	2297	Orange Yellow
G06	0.5743	0.4174	1777	Orange
G08	0.5803	0.4121	1744	Orange
G10	0.5779	0.4146	1757	Orange

(x, y) of glasses were in the range of 0.5111 ~ 0.5910 and 0.4043 ~ 0.4374, the all glasses emitted orange color except for glass G04, and the CCTs of all glasses were in the range of 1,713 ~ 2,297. Comparing the data obtained at different excitation wavelengths, there was a big difference, which is mainly due to the interaction between Sm^{3+} and Tb^{3+} ions.

Conclusions

In summary, we have prepared a novel Tb^{3+T}/TSm^{3+} co-doped phosphate glasses with the composition of P_2O_5-SrO-BaO-ZnO doped with 0.5Tb-xEu$_2$O$_3$ (x = 0.2, 0.4, 0.6, 0.8, and 1.0 mol.%). The results suggested that glasses mainly consisted of metaphosphate groups as well as minor of pyrophosphate and orthophosphate groups, the densities of glasses monotonically increased with the increased Sm_2O_3 content, while the molar volume was the opposite. From the absorption spectra, eight obvious absorption bands were found, which can be assigned to the electron transition from ground level to excited levels. the emission spectra of all glasses excited by 402 nm xenon lamp showed four obvious peaks, and there was no energy transfer between Tb^{3+} and Sm^{3+}. However, the emission spectra of all glasses excited by 374 nm xenon lamp showed nine obvious peaks, and they were attributed to the transitions of Tb^{3+} and Sm^{3+}. Compared with the fluorescence lifetimes obtained under 402 nm light excitation, they had the same variation tendency, but the maximum of fluorescence lifetime was slightly greater. In addition, all glasses emitted orange color based on the CIE chromaticity diagram. Given all that, this systematic study would provide a guidance for preparing orange light emitting glass, and we believe this system glass will have a potential application in display devices.

Acknowledgements

This work has been supported by the Project of Technology Promotion and Industrialization for Key Basic Materials in China (No. 2017YFB0310200), the Scientific Research Foundation of Jiangxi University of Science and Technology (205200100425), the National Natural Science Foundation of China (No. 51672310, No. 51272288) and the Scientific Research Foundation for Universities from the Education Bureau of Jiangxi Province (GJJ190475).

Conflict of Interest

The authors declare no conflict of interest.

References

1. E.F. Schubert, and J.K. Kim, Science 308[5726] (2005) 1274-1278.
2. S.F. Liu, H. Ming, J. Cui, S.B. Liu, W.X. You, X.Y. Ye, Y.M. Yang, H.P. Nie, and R.X. Wang, J. Phys. Chem. C 122[28] (2018) 16289-16303.
3. M.Y. Ding, J.J. Hou, Y.J. Yuan, W.F. Bai, C.H. Lu, J.H. Xi, Z.G. Ji, and D.Q. Chen, Nanotechnol. 29 (2018) 345704.
4. H. Ming, S.F. Liu, L.L. Liu, J.Q. Peng, J.X. Fu, F. Du, and X.Y. Ye, Acs Appl. Mater. Inter. 10[23] (2018) 19783-19795.
5. J. Zhang, X.T. Tao, C.M. Dong, Z.T. Jia, H.H. Yu, Y.Z. Zhang, Y.C. Zhi, and M.H. Jiang, Laser Phys. Lett. 6[5] (2009) 355-358.
6. G.H. Chen, L.Q. Yao, H.J. Zhong, and S.C. Cui, J. Lumin. 178 (2016) 6-12.
7. J.T. Zhao, L.H. Huang, T.Y. Liang, S.L. Zhao, and S.Q. Xu, J. Lumin. 205 (2019) 342-345.
8. B. Afef, M.M. Alqahtani, H.H. Hegazy, E. Yousef, K. Damak, and R. Maâlej, J. Lumin. 194 (2018) 706-712.
9. L. Yuliantini, M. Djamal, R. Hidayat, K. Boonin, P. Yasaka, E. Kaewnuam, and V. Venkatramu, J. Kaewkhao, J. Lumin. 213 (2019) 19-28.
10. N. Wantana, E. Kaewnuam, Y. Ruangtaweep, D. Valiev, S. Stepanov, K. Yamanoi, H. J. Kim, and J. Kaewkhao, Phys. Chem. 164 (2019) 108350.

11. M. Kuwik, A. Górny, J. Pisarska, and W.A. Pisarski, Mater. Lett. 254 (2019) 62-64.
12. R.O. Omrani, S. Krimi, J.J. Videau, I. Khattech, A. El Jazouli, and M. Jemal, J. Non-Cryst. Solids 390 (2014) 5-12.
13. R.J. Yang, H.L. Liu, Y.H. Wang, W.L. Jiang, X.P. Hao, J. Zhan, and S.Q. Liu, J. Alloy Compd. 513 (2012) 97-100.
14. H.J. Zhong, G.H. Chen, L.Q. Yao, J.X. Wang, Y. Yang, and R. Zhang, J. Non-Cryst. Solids 427 (2015) 10-15.
15. N. Kerkouri, M. Haddad, M. Et-tabirou, A. Chahine, and L. Laânab, Physica B 406[17] (2011) 3142-3148.
16. K. Meyer, J. Non-Cryst. Solids 209[3] (1997) 227-239.
17. Y.M. Moustafa, and K. El-Egili, J. Non-Cryst. Solids 240[1-3] (1998) 144-153.
18. L. Han, J.L. Liu, C.W. Lin, H. Gui, J. Song, Q. Zhang, C. Li, Z.W. Luo, T.Y. Liu, and A.X. Lu, Ceram. Int. 45[2] (2019) 2036-2043.
19. B. Colovic, V. Jokanovic, and N. Jovic, Sci. Sinter. 45[3] (2013) 341-350.
20. L. Han, C. Li, C.W. Lin, J.L. Liu, J.Q. Wu, H. Gui, Q. Zhang, Z.W. Luo, T.Y. Liu, and A.X. Lu, J. Am. Ceram. Soc. 102[7] (2019) 4213-4225.
21. R.K. Brow, J. Non-Cryst. Solids 263 (2000) 1-28.
22. E. Ebrahimi and M. Rezvani, Spectrochim. Acta A 190 (2018) 534-538.
23. C.W. Lin, J.L. Liu, L. Han, H. Gui, J. Song, C. Li, T.Y. Liu, and A.X. Lu, J. Non-Cryst. Solids 500 (2018) 235-242.
24. H. Algarni, M. Reben, S. Almoeed, R. Maâlej, and E.S. Yousef, Optik 160 (2018) 340-347.
25. Y. Chen, G.H. Chen, X.Y. Liu, C.L. Yuan, and C.R. Zhou, Opt. Mater. 73 (2017) 535-540.
26. M.E. Alvarez-Ramos, J. Alvarado-Rivera, M.E. Zayas, U. Caldiño, and J. Hernández-Paredes, Opt. Mater. 75 (2018) 88-93.
27. X.Q. Zhou, G.F. Ju, T.S. Dai, Y. Li, H.Y. Wu, Y.H. Jin, and Y.H. Hu, J. Lumin. 218 (2020) 116820.
28. J. Pisarska, A. Kos, M. Sołtys, A. Górny, E. Pietrasik, and W.A. Pisarski, J. Lumin. 195 (2018) 87-95.
29. M.B. Xie, G.X. Zhu, L.H. Zeng, F.F. Xie, C.Y. Liang, and X.P. Zhou, Int. J. Appl. Ceram. Tec. 12[4] (2015) 750-754.
30. A.F.A. Mohammed, G. Lakshminarayana, S.O. Baki, K.A. Bashar, I.V. Kityk, and M.A. Mahdi, Opt. Mater. 86 (2018) 387-393.
31. L.Q. Yao, G.H. Chen, T. Yang, Y. Luo, and Y. Yang, J. Alloy Compd. 692 (2017) 346-350.
32. N. Deopa, S. Kaur, A. Prasad, B. Joshi, and A.S. Rao, Opt. Laser Technol. 108 (2018) 434-440.